Supplementary Information (SI) for Journal of Materials Chemistry A.

Overcoming the mobility penalty introduced by dipole disorder in small-molecule HTM films

Supplementary Information

Benjamin Vella[†a] , Miriam H. Fsadni[†b], Thomas Pope[b], Marcin Giza[a], Fraser J. Angus[a], Ivan Shmarov[a], Paula L. Lalaguna[a], Michele Cariello[a], Claire Wilson[a], Malcolm Kadodwala[a], Thomas J. Penfold*[b], Pablo Docampo*[a], and Graeme Cooke*[a]

[a]School of Chemistry, Joseph Black Building, University of Glasgow, Glasgow G12 8QQ, UK

[b]Chemistry, School of Natural and Environmental Sciences, Newcastle University, Newcastle upon Tyne, NE1 7RU, UK

Table of Contents

1. Synthesis

All reagents were purchased from commercial sources and used as received. Dry solvents were obtained from a Pure Solv 500 MD™ solvent purification system or purchased from Merck. All reactions were performed under nitrogen atmosphere. Brine, in this context, refers to a saturated solution of sodium chloride. Column chromatography was carried out using 60 Å silica gel purchased from Fluorochem/Doug Discovery®. Merck silica gel (60 Å) covered aluminium plates (F254) were used for thin layer chromatography.

4,4'-Dimethoxy-4''-nitrotriphenylamine[1]

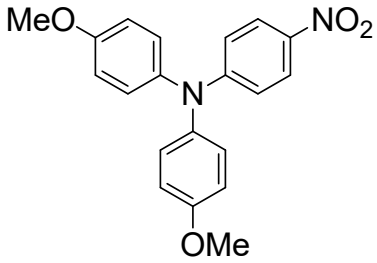

4-Nitroaniline (410 mg, 2.97 mmol), 1-methoxy-4-iodobezene (1458 mg, 6.23 mmol), copper powder (184.9 mg, 2.91 mmol), potassium carbonate (862.4 mg, 6.24 mmol), and 18-crown-6 (31.7 mg, 0.12 mmol) were added to a round-bottomed flask. The reagents were dissolved in DMF (5 mL). The mixture was stirred vigorously under reflux (150°C) for 16 hours. The mixture was then allowed to cool to room temperature and was then diluted with ethyl acetate and extracted with H_2O and brine. The organic layer was dried over $MgSO_4$, filtered, and the solvent was then removed under vacuum. The product was further purified by column chromatography (30% diethyl ether/petroleum ether), and then recrystallised from isopropanol to yield red crystals of the pure product (690 mg, 67%). Melting point: 132 – 134°C (lit.[2,3] 125 – 129°C). R_f = 0.37 (30% diethyl ether/petroleum ether). ^{1}H-NMR ($CDCl_3$, 400MHz) δ = 7.93 (dt, *J* = 9.36, 3.28 Hz, 2H), 7.07 (dt, *J* = 8.96, 2.24 Hz, 4H), 6.84 (dt, *J* = 9.00, 2.28 Hz, 4H), 6.69 (dt, *J* = 9.36, 2.16 Hz, 2H), 3.75 (s, 6H) ppm.

4-Amino-4',4''-dimethoxytriphenylamine[1]

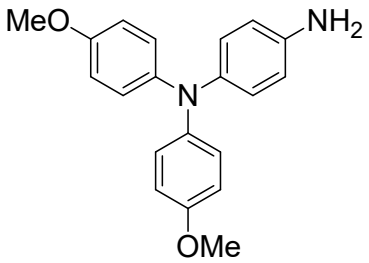

4,4'-Dimethoxy-4''-nitrotriphenylamine (404 mg, 1.15 mmol), 10% palladium on carbon (41.3 mg, 0.388 mmol) and hydrazine hydrate (0.39 ml, 8.07 mmol) were added to a round-bottomed

flask. The reagents were dissolved in dry THF (10 mL). The mixture was vigorously stirred under reflux (66°C) for 24 hours, causing the solution to lose its dark red colour. The reaction mixture was cooled to room temperature after which it was filtered through a short pad of celite to remove the palladium catalyst. Ethyl acetate was used to collect washings from the flask. The product was then recrystallised from H_2O and collected as grey crystals (350 mg, 95% crude yield). The entire yield was used immediately for the final condensation step, due to its instability in air which was observed during NMR sample preparation The colourless solution gradually turned dark grey when exposed to the air for a short period of time. R_f = 0.1 (30% diethyl ether/petroleum ether). ^{1}H-NMR ($CDCl_3$, 400MHz) δ = 6.95 (dt, *J* = 9.04, 2.24 Hz, 4H), 6.87 (dt, *J* = 8.68, 2.12 Hz, 2H), 6.76 (dt, *J* = 9.04, 2.32 Hz, 4H), 6.60 (dt, *J* = 8.68, 2.12 Hz, 2H), 3.77 (s, 6H) ppm.

3,4-Ethylenedioxythiophene-2,5-dicarbonyl chloride[1]

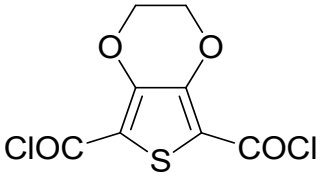

3,4-Ethylenedioxythiophene-2,5-dicarboxylic acid (300 mg; 1.30 mmol) was dissolved in THF (25 mL). DMF (0.01 mL; 0.14 mmol) was added. Thionyl chloride (0.23 mL, 3.12 mmol) was then added dropwise, causing the evolution of fumes and a colour change from a white suspension to a clear yellow solution. After heating the solution at 80°C for 2 hours with vigorous stirring, the solution was left to cool down to room temperature. The remaining thionyl chloride and THF were removed under vacuum, yielding the product acid chloride as a pale, yellow solid. The product was used immediately in the next step without purification, due to its sensitivity to moisture, causing hydrolysis back to the dicarboxylic acid starting material.

N^5,N^7-Bis(4-(bis(4-methoxyphenyl)amino)phenyl)-2,3-dihydrothieno[3,4-][1,4]dioxine-5,7-dicarboxamide (EDOT-Amide-TPA, 1)[1]

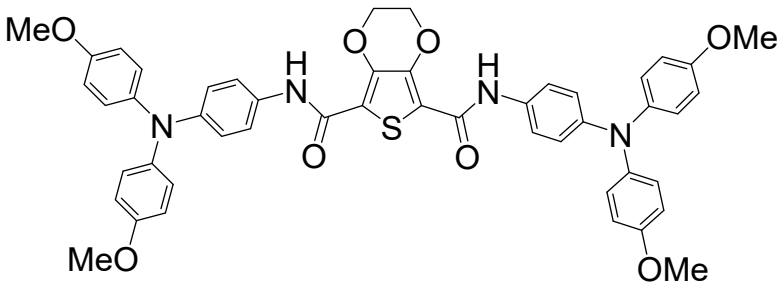

4-Amino-4',4''-dimethoxytriphenylamine (914.4 mg, 2.85 mmol) was dissolved in THF (10 mL) and transferred to a flask containing 3,4-ethylenedioxythiophene-2,5-dicarbonyl chloride (363.2 mg, 1.36 mmol). Triethylamine (0.44 mL, 3.13 mmol) was added, causing the evolution of fumes and the formation of an orange precipitate. The reaction mixture was heated under reflux (66°C) while stirring vigorously for 1 hour. Heating was removed and the reaction mixture was cooled to room temperature overnight. The reaction mixture was filtered under vacuum to collect the orange precipitate, which was washed with 1:1 MeOH/H_2O (10 mL) and cold THF (10 mL). A final wash with petroleum ether (5 mL) was used to remove residual THF. The product was then dried and collected as a yellow powder (790 mg, 70%). Melting point: 300 – 302°C. R_f = 0.27 (30% EtOAc/petroleum ether). ^{1}H-NMR ($CDCl_3$, 400MHz) δ = 8.36 (s, 2H), 7.39 (dt, *J* = 8.96, 1.96 Hz, 4H), 6.99 (dt, *J* = 8.96, 2.16 Hz, 8H), 6.91 (dt, J = 8.92, 1.96 Hz, 4H), 6.60 (dt, *J* = 9.00, 2.24 Hz, 8H), 4.54 (s, 4H), 3.79 (s, 12H) ppm; ^{13}C-NMR (DMSO-d_6, 101MHz) δ = 155.35, 140.50, 125.83, 121.63, 120.88, 114.91, 55.23 ppm; FTIR: v(cm^{-1}): 3369 (weak), 2832 (very weak), 1662 (medium), 1600 (medium), 1537 (medium), 1498 (strong), 1372 (weak), 1233 (strong), 1094 (medium), 1032 (medium), 822 (broad, medium); HRMS (ESI$^+$): m/z calculated for $C_{48}H_{42}N_4O_8S^+$ $[M+H]^+$: 835.2616; found: 835.2807.

N^5,N^7-bis(4-(bis(4-methoxyphenyl)amino)phenyl)-N^5,N^7-dimethyl-2,3-dihydrothieno[3,4-b][1,4]dioxine-5,7-dicarboxamide (DEDOT-Amide-TPA, 2)

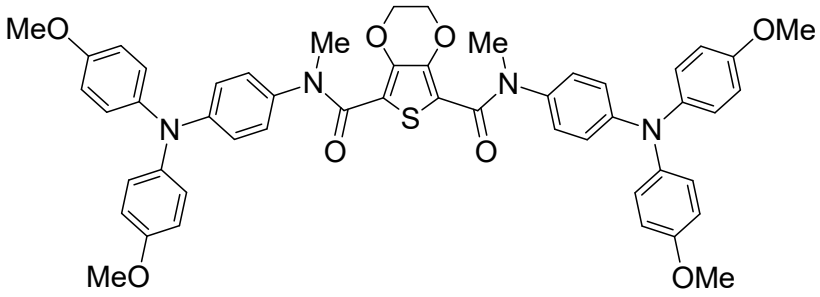

EDOT-Amide-TPA (1016 mg, 1.22 mmol) and sodium hydride (60% in mineral oil, 278 mg, 6.95 mmol) were dissolved in DMF (15 mL). The reaction mixture was heated at 130°C for 2 hours, causing the reactants to dissolve, forming a red solution. The mixture was then allowed to cool down to around 40°C after which iodomethane (0.23 mL, 3.60 mmol) was added dropwise. This caused the formation of a yellow precipitate in the flask. The reaction was left to stir at 40°C overnight. After reaction completion, product was precipitated by the

addition of petroleum ether (30 mL). The crude product was collected by vacuum filtration as a pale green powder and was purified by column chromatography (10% acetone/DCM) to yield the pure product as a yellow solid (507 mg, 48%). Melting point: 200 – 202°C. ^{1}H NMR (400 MHz, $CDCl_3$) δ = 7.06 – 6.98 (8H, m), 6.87 – 6.79 (12H, m), 6.77 – 6.72 (4H, m), 3.96 (4H, s), 3.78 (12H, s), 3.34 (6H, s). ^{13}C NMR (101 MHz, $CDCl_3$) δ 162.43, 156.17, 148.14, 140.80, 140.59, 135.71, 128.00, 126.79, 120.25, 114.90, 114.55, 64.49, 64.14, 55.57, 53.54, 38.44, 25.47. FTIR: v(cm^{-1}): 3041 (very weak), 2946 (weak), 2899 (weak), 2829 (weak), 1634 (strong), 1604 (medium), 1500 (strong), 1235 (strong), 1092 (strong), 1031 (strong), 815 (strong). HRMS (ESI^+): m/z calculated for $C_{50}H_{46}N_4O_8S^+$ $[M+H]^+$: 863.9872; found: 863.3104.

Thiophene-3,4-dicarbonyl dichloride[4]

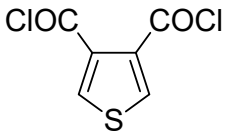

Thiophene-3,4-dicarboxylic acid (2.48 g, 14.43 mmol) was dissolved in dry THF (20 mL) and DMF (0.022 mL, 0.28 mmol) was added. Thionyl chloride (2.42 mL, 33.19 mmol) was added dropwise, causing the starting material to dissolve into a yellow solution. The solution was degassed with nitrogen and heated under reflux (80°C) for 2 hours. The solution was then allowed to cool down to room temperature, and the remaining thionyl chloride and solvent were removed under vacuum, yielding the resulting acid chloride as a brown solid (3.02 g crude yield). The product was used without further purification due to sensitivity to moisture, which causes hydrolysis of the acid chloride to yield the dicarboxylic acid starting material.

***N*$_3$,*N*$_4$-bis(4-** **(bis(4-**

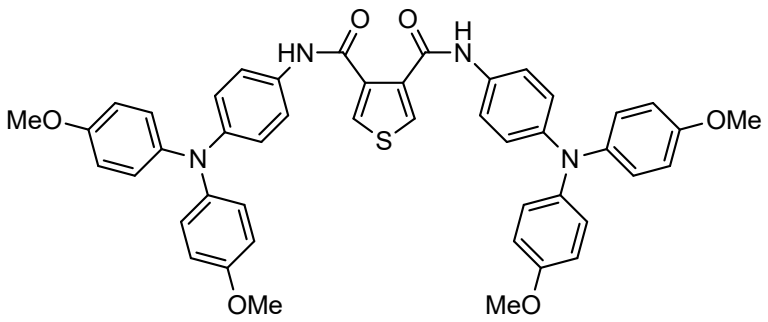

methoxyphenyl)amino)phenyl)thiophene-3,4-dicarboxamide[4]

The total yield of the acid chloride was dissolved in dry THF (20 mL). 4-Amino-4',4''-dimethoxytriphenylamine (9.706 g, 30.29 mmol) was added, followed by triethylamine (4.62 mL, 33.18 mmol) which was slowly added to the solution causing the formation of a dark red solution. The reaction mixture was then heated under reflux for 2 hours. The mixture was allowed to cool to room temperature overnight. The mixture was concentrated under vacuum and diethyl ether (50 mL) was added to precipitate a pale yellow solid. After cooling overnight in the freezer, the precipitate was filtered to give the crude product. The product was purified by column chromatography (10% acetone/DCM) to obtain an amorphous solid, that was then recrystallised from ethanol (100 mL) yielding pale yellow crystals of pure product (2.47 g, 22%). Melting point 232 – 234°C. ^{1}H NMR (400 MHz, $CDCl_3$) δ = (400 MHz, $CDCl_3$) 10.20 (2H, s), 7.94 (2H, s), 7.56 (4H, dt), 7.06 (8H, dt), 6.98 (4H, dt), 6.85 (8H, dt), 3.82 (12H, s). ^{13}C NMR (101 MHz, DMSO) δ = 161.74, 155.13, 144.23, 140.70, 137.34, 137.05, 132.61, 130.47, 128.89, 128.20, 125.48, 125.31, 121.51, 121.09, 114.83, 55.21, 54.91, 21.04. FTIR: ν(cm^{-1}): 3258 (very weak), 3100 (very weak), 3037 (weak), 2941 (weak), 2829 (weak), 1605 (strong), 1557 (medium), 1536 (weak), 1500 (strong), 1464 (medium), 1441 (weak), 1313 (weak), 1235 (strong), 1175 (medium), 1104 (medium), 1031 (strong), 892 (weak), 824 (strong), 779 (medium), 716 (medium), 632 (weak), 617 (weak), 572 (medium). HRMS (ESI^+): m/z calculated for $C_{46}H_{40}N_4O_6S^+$ ($M+H^+$) = 777.2669; found = 777.2744.

2. High-Resolution Mass Spectra

All high-resolution mass spectra were obtained using an Agilent 6546 Q-TOF-MS high resolution accurate mass spectrometer, from powder samples of our amide HTMs dissolved in ethyl acetate.

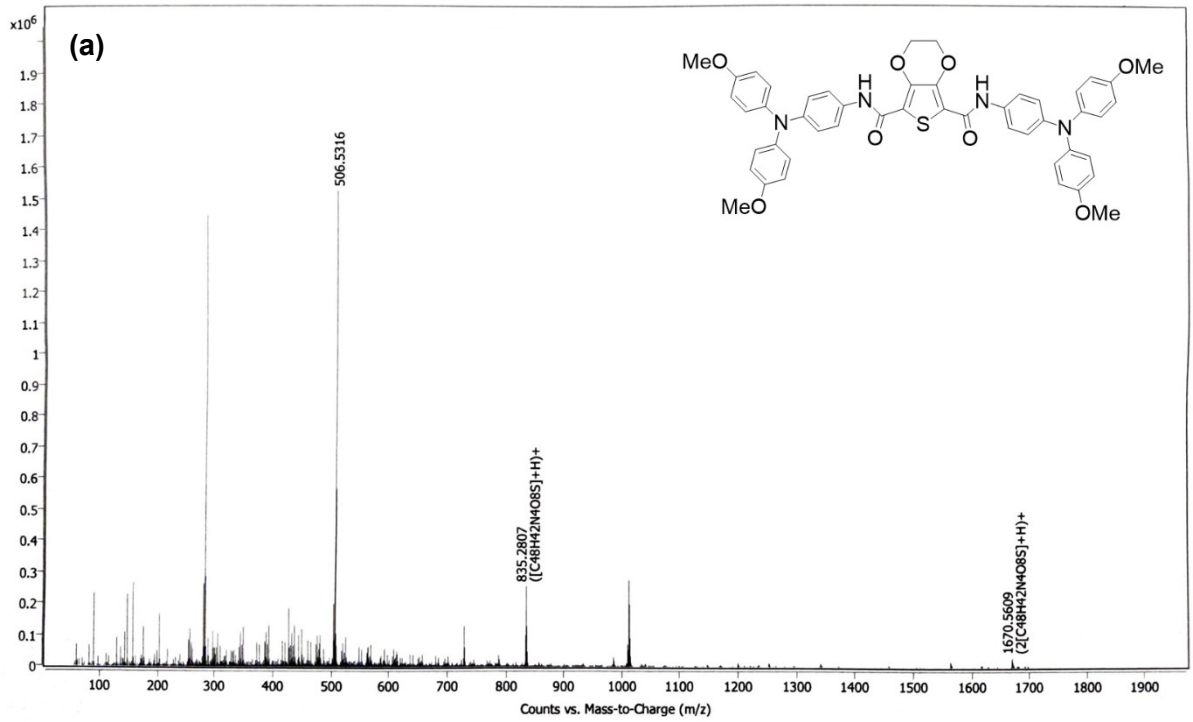

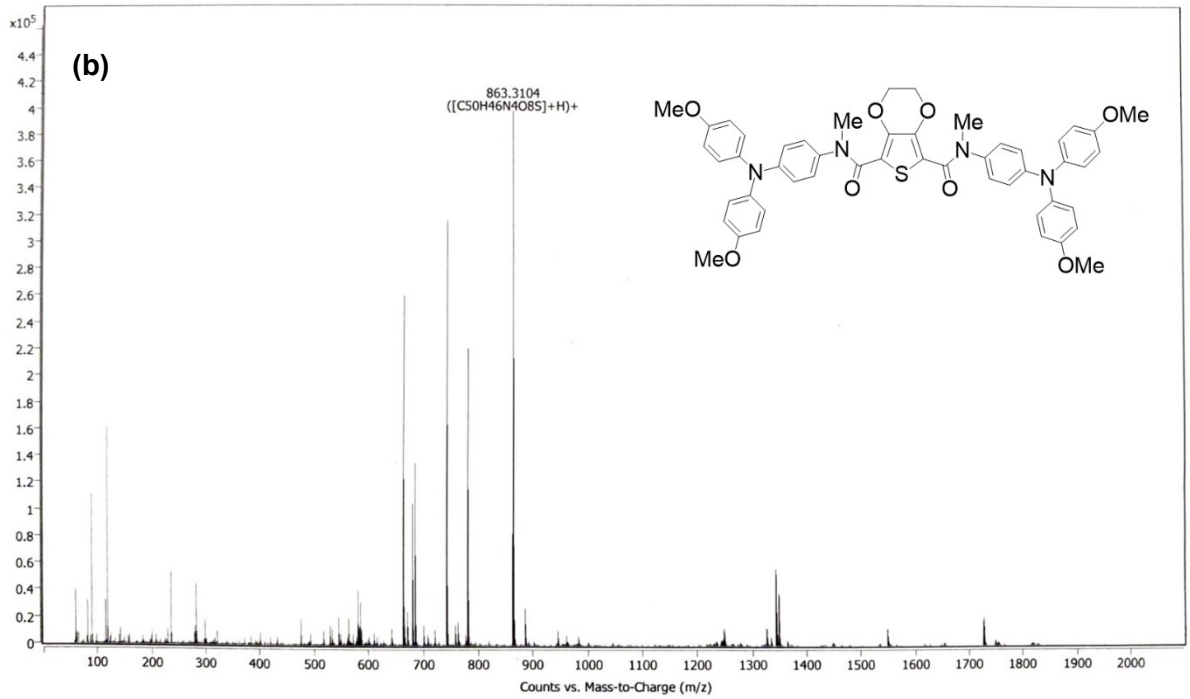

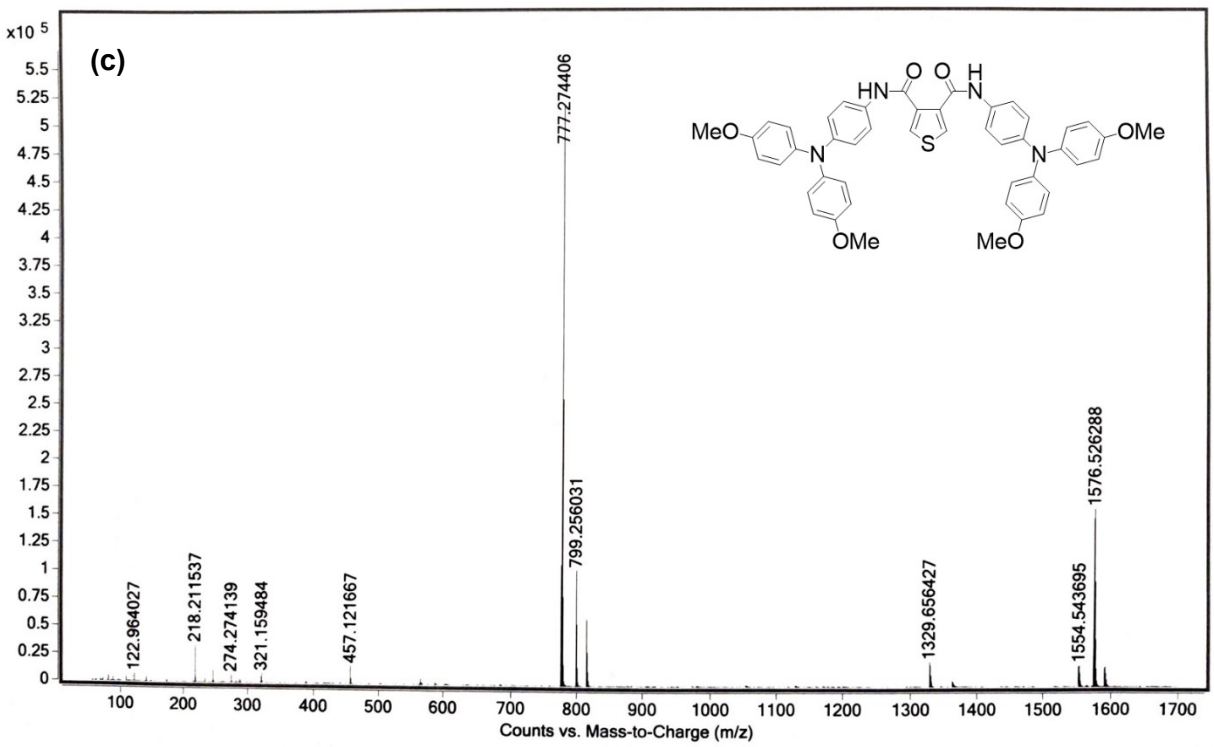

Figure S1: High-resolution mass spectra of (a) EDOT-Amide-TPA (**1**), (b) DEDOT-Amide-TPA (**2**) and (c) TPABT (**3**)

3. NMR Spectroscopy

Characterisation of Amide HTMs

^{1}H and ^{13}C NMR spectra were acquired using a Bruker AVIII 400 MHz spectrometer, with $CDCl_3$ as a solvent. All chemical shift values are reported in ppm relative to tetramethylsilane (TMS), and are referenced to the residual solvent peaks.

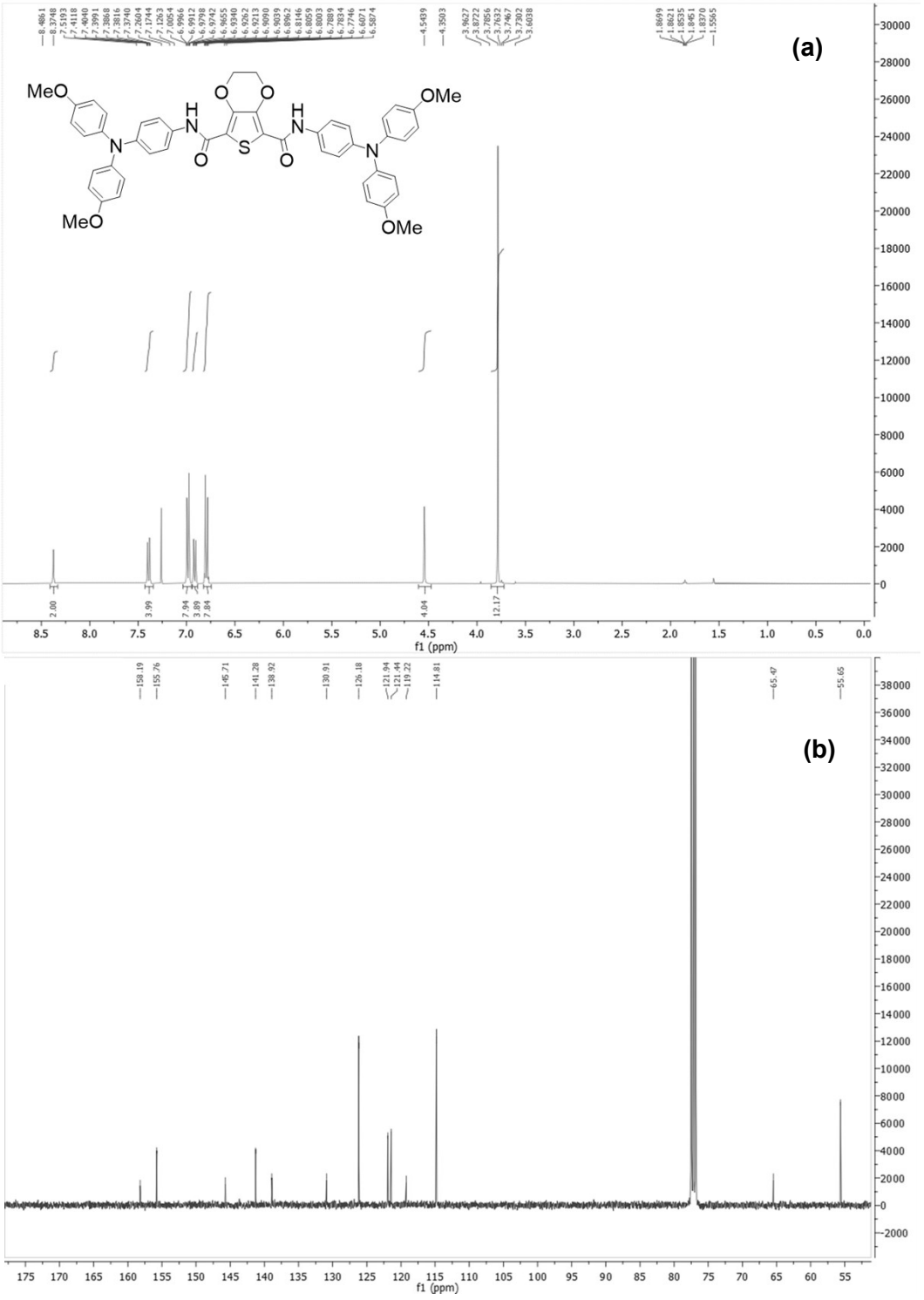

Figure S2: (a) ^{1}H-NMR and (b) ^{13}C-NMR spectra of EDOT-Amide-TPA (**1**).

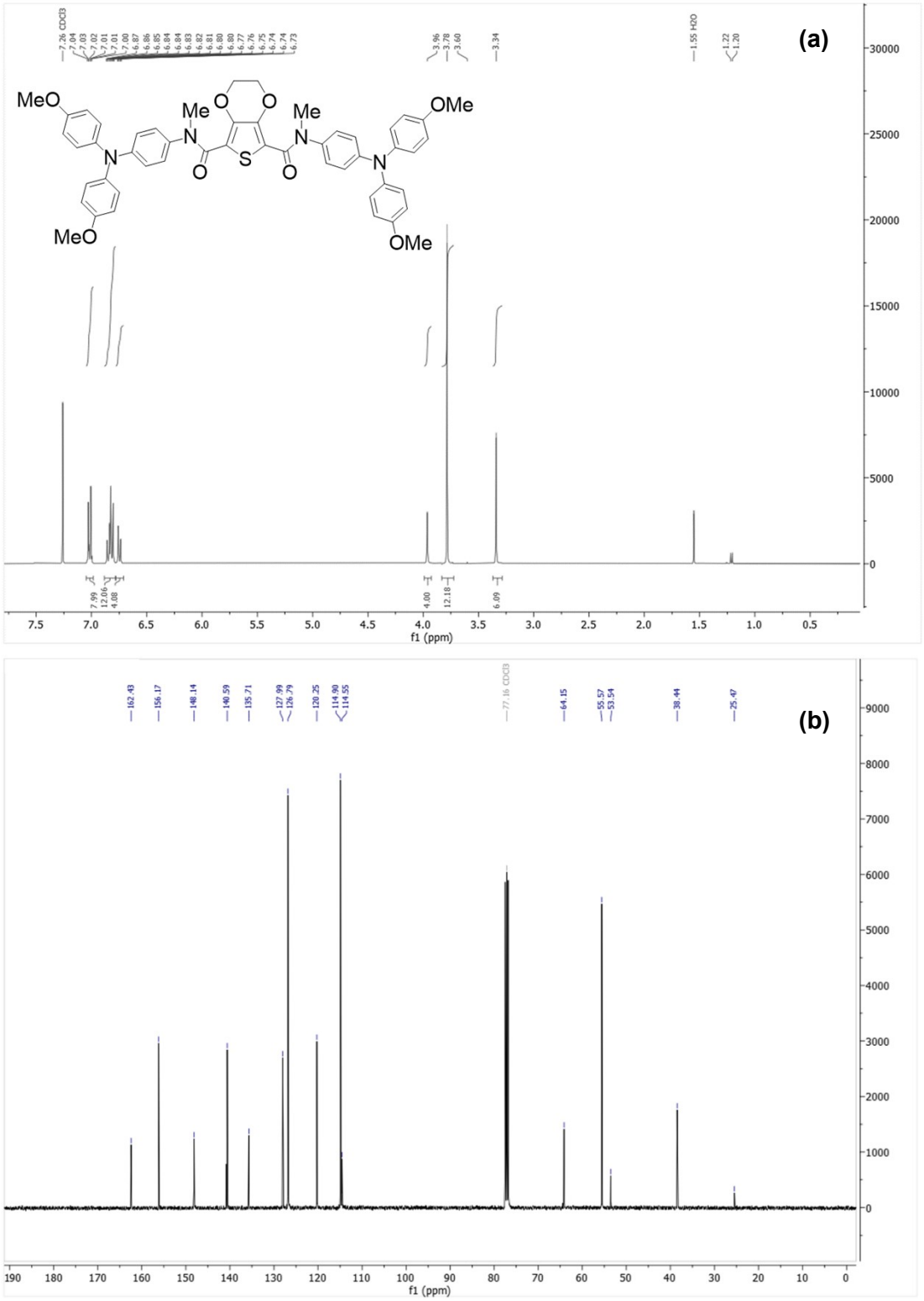

Figure S3: (a) ^{1}H-NMR and (b) ^{13}C-NMR spectra of DEDOT-Amide-TPA (**2**).

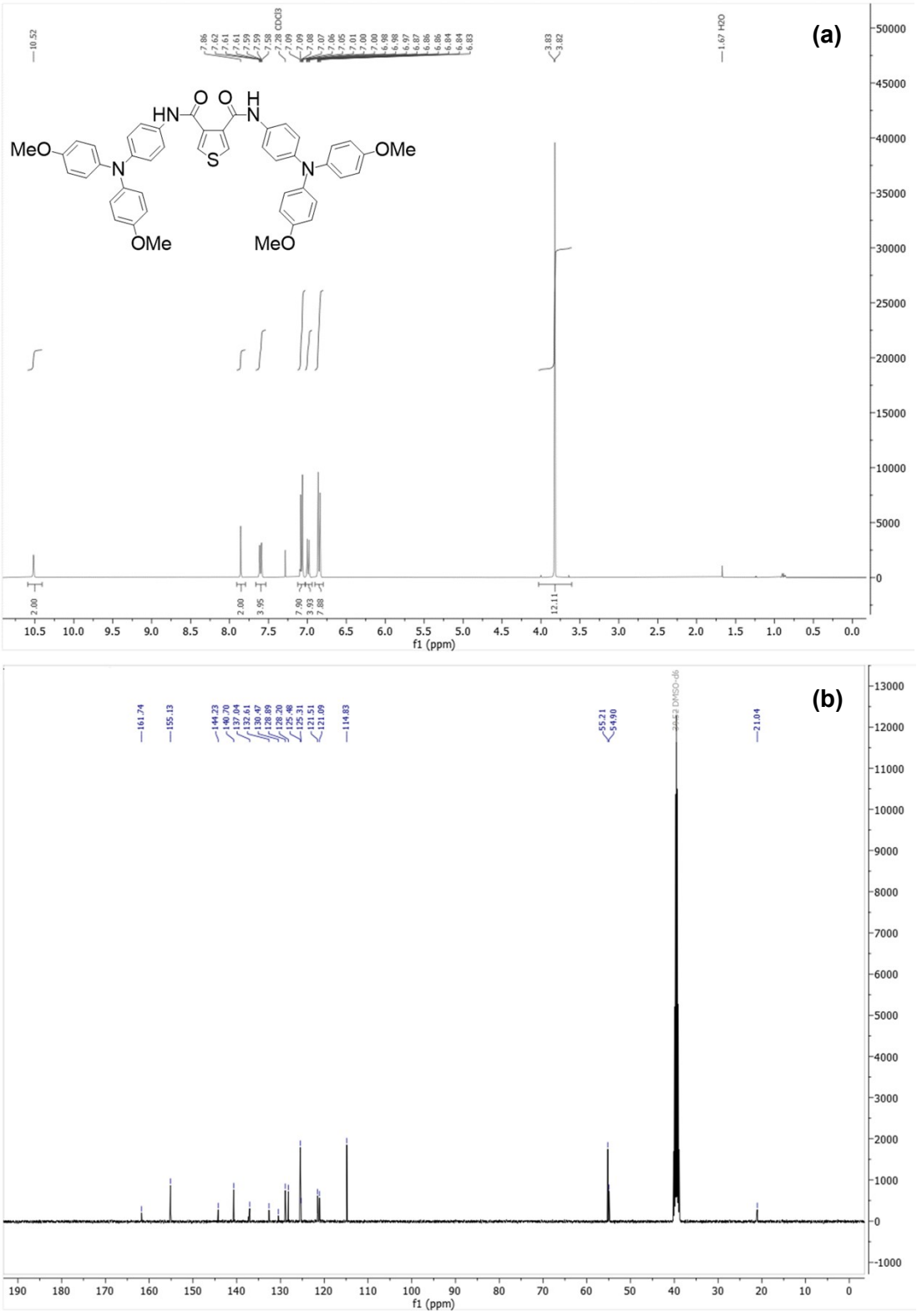

Figure S4: (a) ^{1}H-NMR and (b) ^{13}C-NMR spectra of TPABT (**3**).

Supplementary NMR studies

For VT-NMR studies, ^{1}H-NMR spectra were recorded as before at three temperatures by first cooling the samples to 0°C, then heating back up to room temperature, then 50°C. Samples were left to equilibrate at the desired temperature for 5 minutes prior to acquisition. Solutions of our HTMs were prepared by dissolving 10 mg of HTM in 0.6 mL $CDCl_3$, thus yielding solutions at a concentration of 20 mM for compound **1**, 19.3 mM for compound **2**, and 21.5 mM for compound **3**.

For the DMSO-d6 titrations, solutions with similar concentrations as above were prepared, as well as a stock solution of DMSO-d6 in $CDCl_3$ to allow for the gradual addition of DMSO-d6 into the NMR solution. The HTM solutions above are of sufficient concentration to not be significantly diluted by the addition equivalents of DMSO-d6 from the stock solution, to minimise dilution effects in the NMR spectrum.

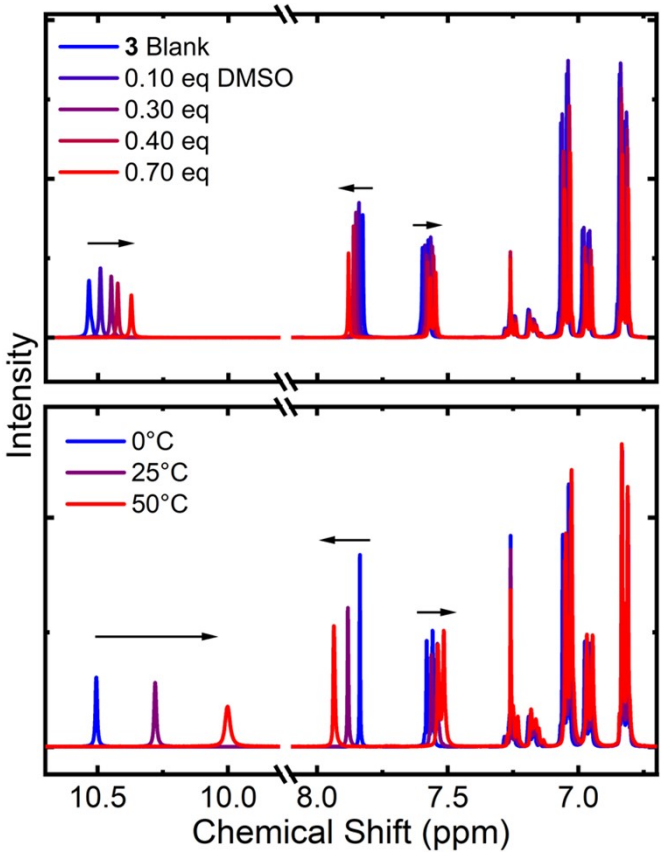

Figure S5: Partial NMR spectra showing the aromatic and amide proton region in compound **3**, (a) with increasing concentration of DMSO-d6, (b) with increasing temperature.

4. Cost Analysis

The synthetic cost of our amide HTMs was estimated based on the experimental amounts given in Section 1 above. We used procedures published by Osedach, *et al*. and Petrus, *et al*. to estimate the materials cost based off of online prices obtained from Merck as our primary supplier.[1,5,6] Prices in USD have been converted from GBP due to our location, using an exchange rate of £1 = $1.28 as of 29/05/2024. Therefore the total costs given below are subject to change depending on availability and demand, as well as fluctuations in currency value.

The material cost of spiro-OMeTAD has previously been reported to lie around $91 / g.[3,7]

EDOT-Amide-TPA

Compound	Mass used (kg)	Cost per kg ($)	Material cost ($)
EDOT-COOH	0.000300	5455.36	1.64
DMF	0.00000950	5.09	0.000048
$SOCl_2$	0.000377	27.67	0.01
THF	0.0178	9.24	0.16
TPA-NH_2 [3]	0.000914	2280.00	2.08
Triethylamine	0.000316	21.54	0.01
THF (solvent)	0.00888	9.24	0.08
MeOH (wash)	0.00396	2.21	0.01
THF (wash)	0.00888	9.24	0.08
Petroleum ether (wash)	0.00320	142.40	0.46
		Total	$4.53
		Yield	0.79 g
		Total Material Cost	**$5.74 / g**

DEDOT-Amide-TPA

Compound	Mass used (kg)	Cost per kg ($)	Material cost ($)
EDOT-Amide-TPA	0.00102	5455.36	5.54
NaH 60%	0.000278	231.68	0.064
DMF	0.0143	5.09	0.073
CH_3I	0.000524	154.94	0.081
Petroleum ether (precipitation)	0.0192	142.40	2.73
Acetone (Purification)	0.0791	83.98	6.64
Dichloromethane (Purification)	1.325	11.16	14.79
		Total	$8.49
		Yield	0.507 g
		Total Material Cost	**$16.76 / g**

TPABT

Compound	Mass used (kg)	Cost per kg ($)	Material cost ($)
Thiophene-COOH	0.00248	3120.00	7.74
$SOCl_2$	0.000278	231.68	0.064
DMF	0.0000209	5.09	0.00011
THF	0.0178	154.94	2.75
TPA-NH_2 [3]	0.00971	83.98	0.82
Triethylamine	0.00337	11.16	0.038
THF (solvent)	0.0178	9.24	0.16
Diethyl ether (precipitation)	0.0353	142.40	5.03
Ethanol (Recrystallisation)	0.0789	2.78	0.22
Acetone (Purification)	0.0791	83.98	6.64
Dichloromethane (Purification)	1.325	11.16	14.79
		Total	$38.25
		Yield	2.47 g
		Total Material Cost	**$15.48 / g**

5. Fourier Transform Infrared Spectroscopy (FTIR)

All FT-IR spectra for characterisation were recorded on a Jasco FTIR-4100 spectrometer from neat solids. To compare the FTIR spectra of amorphous films compared to crystals, films were spin coated on glass following similar methodology to that described in the Conductivity Measurements section below. Far more concentrated solutions were used where possible, and a larger substrate was employed to deposit a film of sufficient thickness to facilitate collection. Films were then removed from the glass surface by scraping with a clean and dry razor. Single crystals were grown using the same methods as for single crystal X-ray crystallography. The FTIR spectra of the dry powder or crystal was then recorded.

6. Thermochemistry

TGA was performed using a TA Instruments SDT Q600 V8.3 thermogravimetric analyser. Decomposition of the samples was taken to begin when > 5% of the mass of the sample is lost. DSC was performed on a TA Instruments DSC2A-01781. Samples were subjected to three heating and cooling cycles for DSC, ensuring that the heating did not exceed 10°C below their decomposition temperature determined from TGA. All the thermal analyses were carried out under N_2, at a rate of 10°C per minute.

7. Computational Analysis

a. Density Functional Theory

Density functional theory (DFT) calculations were performed at the DFT(PBE0)/def2-sv(p) level of theory as implemented within the Orca (v. 5.1) quantum chemistry package.[8] From these calculations all molecular properties, including the Debye dipole moments, were obtained. Consistent with our previous work,[9] calculations were performed both in vacuum and in dichloromethane (DCM), to approximate the effect of the film environment, using the conductor-like polarizable continuum model (C-PCM). Based on a procedure by Chi et al. adapted to calculations performed at the PBE0/def2-sv(p) level,[10] a linear correction factor of –0.206 eV was applied to the HOMO energies for molecules optimised in DCM.

b. Crystal Molecule Pairs: Dipole moments and Binding Energy

While long-range order is generally not observed in the solution-processed HTM thin films, crystal structures may give us an indication of the preferential orientation of molecules and provide a best-case scenario for the intermolecular interactions. The crystal structures of **1** and **3**, show distinct hydrogen-bonded (H-bonded) pairs, and our ^{1}H-NMR and FTIR experiments suggest these may already form in concentrated solutions as well as in the powders (main text, Figures 3, 4 and 9). Molecular pairs forming in solution would remain stable during spin-coating if their binding energy is sufficiently high. Therefore, the binding energies of the molecular pairs extracted from the crystal structure data may further support the presence of these pairs in our amorphous thin films. If the pairs are closely bound, these could act as a single hopping site with an overall dipole moment that is either reduced or enhanced, depending on the relative orientations of the individual molecules. Since a high dipole moment has been shown to quench mobility, the propensity for high dipole materials to exist as stable (hydrogen-bonded) reduced-dipole pairs is expected to significantly enhance the overall mobility and is consistent with the favourable experimental charge transport properties we observe.

Figure S6 shows the different molecule pairs extracted from crystal structure analysis of our amides, with the arrows indicating the relative orientation of monomer EDOT and thiophene cores. Antiparallel molecule orientation is shown using yellow arrows, while parallel and orthogonal orientations are shown using red arrows. Table S1 gives the Debye dipole moments, binding energies and intermolecular distances of the molecule pairs shown in Figure S6, as well as the relative orientation of the molecules involved.

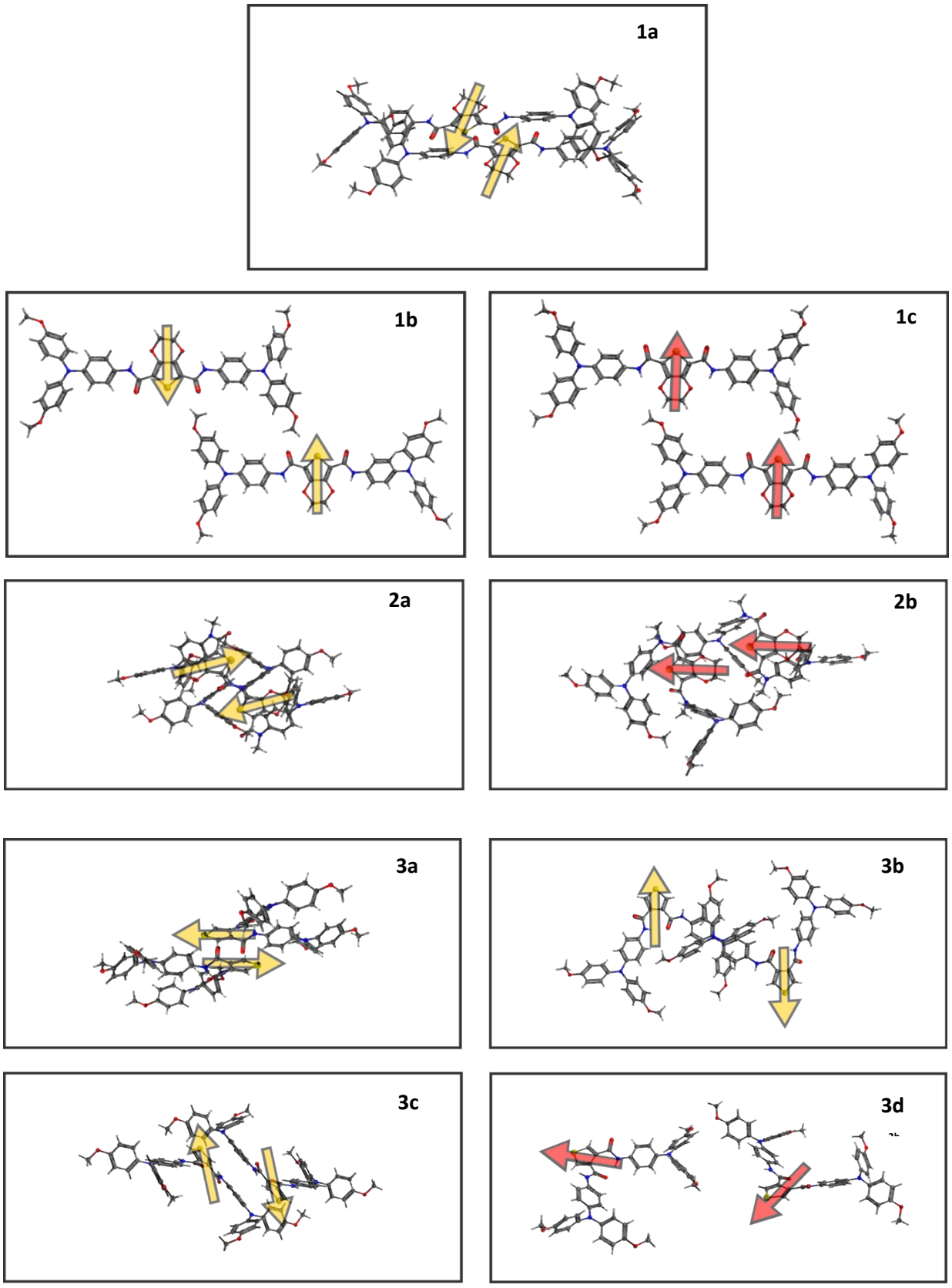

Figure S6: Close-lying molecule pairs extracted from the crystal structures of HTMs **1** (1a-1c), **2** (2a,b) and **3** (3a-d), with arrows showing the relative orientation of their respective cores.

Table S1: Properties of amide pairs extracted from X-ray spectroscopy, shown in Figure S6, with their theoretical dipole moments and binding energies, from DFT (PBE0/def2-sv(p)) calculations in vacuum.

Pair	Orientation	Dipole (D)	Binding Energy (eV)	Intermolecular Distance (Å):		
				Cores	Shortest	TPA N—N
1a	**antiparallel***	**0.0**	**0.86**	**4.0**	**2.7**	**5.0**
1b	antiparallel	0.0	0.31	15.5	2.7	10.9
1c	parallel	21.0	0.29	13.9	2.4	14.8
2a	**antiparallel**	**0.0**	**0.78**	**8.0**	**2.5**	**5.2**
2b	parallel	7.1	0.58	3.7	2.3	9.9
3a	**antiparallel***	**0.0**	**0.84**	**3.6**	**2.1**	**12.1**
3b	antiparallel	0.0	0.36	15.0	2.9	5.0
3c	antiparallel	0.0	0.29	9.7	2.7	9.0
3d	orthogonal	8.6	0.07	19.3	2.9	9.0

* Molecular pair exhibits hydrogen bonding at the amide linkers.

We find that 0 Debye antiparallel pairs with short core-to-core distance have the highest binding energies, between 0.8 and 0.9 eV. If these pairs form in solution, they are likely to remain stable in the film and would lower the energetic disorder. We find that in **3**, antiparallel arrangements (**3a**) of molecules are by far the most stable and parallel pairs are not found. The binding energies of antiparallel pairs (**1a**) is also highest in **1**. However, when the molecules are parallel (**1c**) the overall dipole is greatly enhanced to 21 D. In compound **2**, the difference in binding energies between quenched dipole antiparallel pairs (**2a**) and enhanced dipole parallel 7 D pairs (**2b**) is only 0.2 eV, so that once formed, both are likely to be stable in the film.

It is worth noting that H-bonded antiparallel pairs **3a** and **1a** have short core-to-core distances (~4 Å), enabling them to operate as a single hopping site with a quenched dipole moment. While other configurations in **1** and **3**, exhibit longer core to core distances, they still form short contacts between TPA side units on which the HOMO is located. In **2**, dipole enhanced parallel pairs **2b** have the shortest core-to-core distance, while dipole quenched antiparallel pairs **2a** have short TPA N-N distances.

From these calculations, we find that the proportion of quenched-dipole pairs compared to dipole enhanced pairs is greatest in HTMs **1** and **3**. In a film, **1** would still have an overall more complex potential energy landscape than **3**, since its monomers have a higher dipole moment, which we would expect to reduce the conductivity. In **2**, the difference in the stability of favourably and unfavourably oriented molecular pairs is small, so that the correlated energetic disorder in the film remains high. These results are thus consistent with the trend in the amide conductivities reported in our study, of **3** > **1** >> **2**.

c. Kinetic Monte Carlo simulations

To model the hole transport material, a uniform square lattice of N^3 grid points is set up, to which site energies are assigned. Holes are distributed over the sites randomly to achieve a given hole density, ρ_0, and the energies recalculated. For each step in the simulation, holes are able to hop to vacant neighbouring sites within a radius of $\sqrt{3}L$, where L is the lattice spacing. For each possible hop we find the energy change, ΔE, and associated Marcus hopping rate, which for a hop between sites i and j is given by Equations 1 and 2 respectively,

$$\Delta E_{ij} = \Delta E_{ij}^{corr} + \Delta E_{ij}^{coulomb} + \Delta E_{ij}^{field} \quad (1)$$

$$k_{ij} = \omega_0 e^{-2\gamma|R_{ij}|} \times e^{-(\lambda + \Delta E)^2/4\lambda k_B T} \quad (2)$$

where ω_0 is the hopping attempt frequency, R_{ij} is the spatial vector between the sites and λ is the reorganisation energy.

The free parameters for the simulation are outlined in Table S2 below.

Table S2: List of parameter settings for the kMC calculation.

Parameter	Description	Value	Units
E_{HOMO}	HOMO energy	0.0	eV
E_F	Fermi energy	0.0	eV
ρ_0	Initial charge density	10^{-5}	nm^{-1}
L	Lattice spacing	1	nm
γ	Inverse charge localization	2.0	nm^{-1}
ω_0	Hopping attempt frequency	10^{12}	s^{-1}
ϵ_R	Relative permittivity	3.0	ϵ_0
d_M	Monomer Dipole	5.0	D
d_P	Pair Dipole	0.0	D
N	System Dimensions	200	grid points

In calculating the change in site energies, E_{HOMO} is kept constant over each site, and any variance, E_i^{unc}, was neglected so that the effect of correlated noise on hole mobility could be definitively probed. This simplifies the energy differences between sites, which then only depend on the change in electric field, the coulomb repulsion and correlated noise term. The change in coulomb energy results from the change in the electrostatic interaction of the hole and all other holes in the system on changing site and is given by Equation 3:

$$\Delta E_{ij}^{coulomb} = \frac{1}{\epsilon_r}\left(\sum_{\substack{k \neq j \\ k = occupied}} \frac{1}{|R_{jk}|} - \sum_{\substack{k \neq i \\ k = occupied}} \frac{1}{|R_{ik}|} \right) \quad (3)$$

where ϵ_r is the relative permittivity of the medium.

The correlated disorder term, ΔE_{ij}^{corr}, reflects the energy change due to the interaction of electronic dipole moments on neighbouring sites, and is given by Equation 4.

$$\Delta E_{ij}^{corr} = \frac{1}{\epsilon_r}\left(\sum_{k \neq j} \frac{d_k \cdot R_{jk}}{|R_{jk}|^3} - \sum_{k \neq i} \frac{d_k \cdot R_{ik}}{|R_{ik}|^3} \right) \quad (4)$$

The dipole magnitude is kept constant for all sites and the direction is generated semi-randomly by defining the azimuthal and polar angles, as previously detailed by Pope, *et al*.. For systems with a non-zero pair density, grid point pairs are distributed randomly, and the pair magnitude is set to zero and aligned with the reference frame.

For each hopping event, all possible hopping rates are probabilistically weighted, and an event is chosen at random. The event is executed, the time is added to the total simulation run time and the site energy grid is updated. The simulation is allowed to proceed over 1,000,000 steps, to ensure convergence. For each system, the outputs from 88 simulations are taken to obtain an average mobility.

8. Electrochemistry

All voltammograms were measured on 10^{-4} M solutions of our amides in dry dichloromethane. 6 mL of each solution was used for the measurement, to which tetrabutylammonium hexafluorophosphate was added at a concentration of 0.1 M as an electrolyte. All solutions were thoroughly purged with nitrogen and kept in this inert atmosphere throughout all measurements. Electrodes used were: platinum disc working electrode, platinum wire counter electrode, and a silver wire pseudo-reference electrode. Ferrocene was also used as an external calibrant, and thus the reported spectra were referenced to the Fc^+/Fc redox couple. All electrodes were cleaned before use and between each measurement.

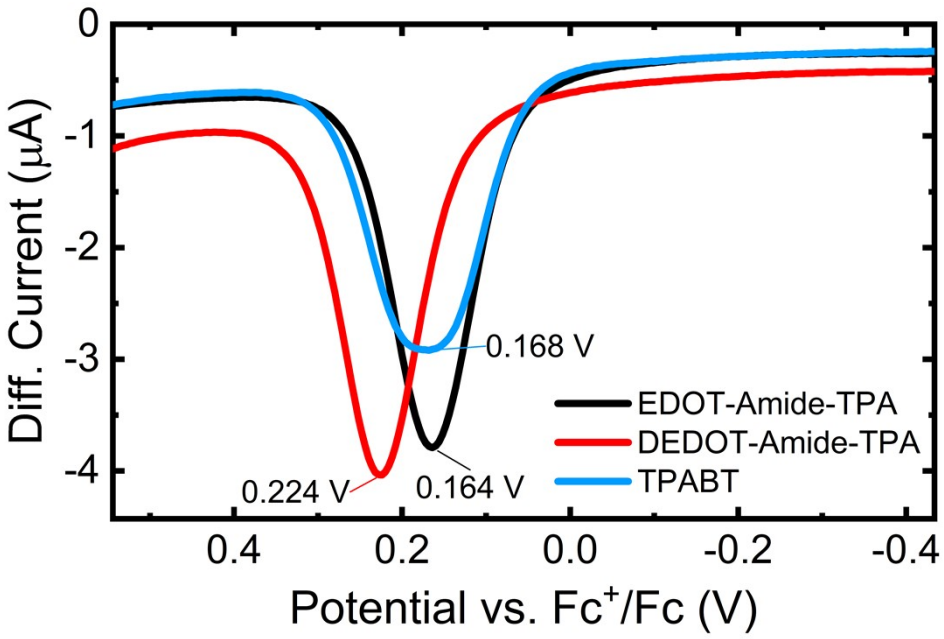

Figure S7: Stacked square wave voltammograms (SWVs) of our amide materials, showing their halfway potentials referenced to ferrocene.

From the halfway potentials in Figure S7, the IPs were estimated using Equation 5:[11]

$$IP = (E_{1/2} \text{ vs. } Fc^+/Fc) + 4.8 \text{ (eV)} \quad (5)$$

9. Single Crystal X-ray Analysis

Single crystals of **2** and **3** were grown via slow evaporation of solutions in chlorobenzene, while crystals of **1** were grown via slow evaporation from a 1:1 dichloromethane:methanol solution. The single crystal structures of **2** and **3** were resolved using the following computational details.

Data collection: *APEX3* Ver. 2016.9-0 (Bruker-AXS, 2016); cell refinement: *SAINT* V8.40B (Bruker, 2016); data reduction: *SAINT* V8.40B (Bruker, 2016); program(s) used to solve structure: SHELXT 2018/2 (Sheldrick, 2018); program(s) used to refine structure: *SHELXL* 2018/3 (Sheldrick, 2015); molecular graphics: Olex2 1.5 (Dolomanov *et al.*, 2009); software used to prepare material for publication: Olex2 1.5 (Dolomanov *et al.*, 2009).

Single crystal structures of **1** were resolved by the UK National Crystallography Service.

Resolved structures were analysed in VESTA 3 software. In order to estimate the different packing behaviour of different amide-based HTMs, the nearest HOMO distance between molecules in the crystal was estimated as the shortest N-N distance between the triphenylamine groups, where the HOMO is mainly situated.

CCDC Deposition numbers are:

EDOT-Amide-TPA (Compound **1**): Deposition Number **2301541**

Unit Cell Parameters: a 55.7783(6) b 55.7783(6) c 10.4905(2) I41/a

DEDOT-Amide-TPA (Compound **2**): Deposition Number **2301539**

Unit Cell Parameters: a 16.6681(5) b 18.0603(6) c 16.6318(5) P21/c

TPABT (Compound **3**): Deposition Number **2301540**

Unit Cell Parameters: a 12.1294(3) b 14.8596(3) c 27.9555(8) P21/c

10. Oxidised HTM titrations

To determine the molar extinction coefficients of our oxidised HTMs, we followed a published procedure[12] and prepared standard solutions of **1**, **2**, **3**, and spiro-OMeTAD in chlorobenzene in volumetric flasks. A standard solution of AgTFSI in chlorobenzene was also prepared. From the AgTFSI stock solution, one mole equivalent of oxidant was titrated into the HTM solutions, causing an immediate colour change. Our amide-based HTMs turned different shades of dark green, while spiro-OMeTAD formed a dark red solution. The resulting UV spectra are shown in Figure S8.

The molar extinction coefficients were then calculated according to the Beer-Lambert law (Equation 6) which equates absorbance to the concentration of the absorbing species:

$$A = \varepsilon\, b\, c \qquad (6)$$

Where A = absorbance, b = path length, and c = concentration.

All estimated molar extinction coefficients are summarised in Table S3.

Table S3:

Species	A_{max}	Concentration (mM)	b (cm)	ε (cm^{-1} M^{-1})
1	0.285	0.0100	1	**28500**
2	0.18	0.0100	1	**18000**
3	0.389	0.0100	1	**38900**
Spiro	0.755	0.0095	1	**79759**
EDOT$^+$TFSI$^-$	0.43	0.0169	1	**25444**
DEDOT$^+$TFSI$^-$	0.129	0.0114	1	**11316**
TPABT$^+$TFSI$^-$	0.363	0.0127	1	**28583**
Spiro$^+$TFSI$^-$	0.651	0.0184	1	**35380**

Calculated molar extinction coefficients of all oxidised HTMs used in this study, from the results of our AgTFSI titrations.

From the known molar extinction coefficients of all of our HTMs, we derive Equation 7 for the ratio of oxidised species in our doped HTM films, expressed as a percentage:

$$c = \frac{A}{\varepsilon b}$$

$$c_{unox} = \frac{A_{unox}}{\varepsilon_{unox} b} \qquad c_{ox} = \frac{A_{ox}}{\varepsilon_{ox} b}$$

$$\%oxidation = \frac{c_{ox}}{c_{unox}} \times 100$$

$$= \frac{A_{ox} / \varepsilon_{ox} b}{A_{unox} / \varepsilon_{unox} b} \times 100$$

The path length in this case is the film thickness through which the UV-Visible beam passes through. It is equal for both oxidised and unoxidised species and so is cancelled out.

$$\%\ oxidation = \frac{A_{ox} \varepsilon_{unox}}{A_{unox} \varepsilon_{ox}} \times 100 \qquad (7)$$

This equation was used to estimate the extents of oxidation of our doped HTM films as measured through film UV absorption spectroscopy. The calculated values were then used to compare the conductivity measurements of different HTMs on the same axes.

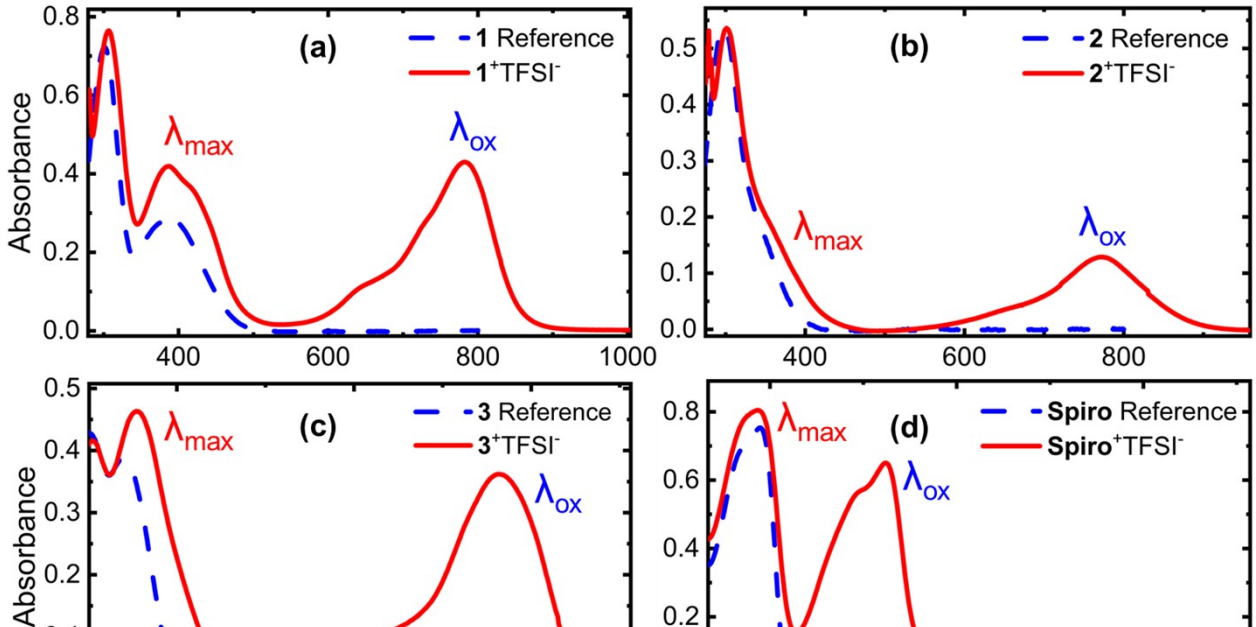

11. Conductivity Measurements

a. Substrate Preparation

Patterned indium-tin oxide substrates (ITO) on glass were prepared for conductivity measurements by etching with a Rofin EasyMark IV F20 laser etcher. A channel was etched on the conductive substrate across which the conductivity of our materials could be measured. Since organic semiconductors in their pristine state exhibit very low conductivity, two different channel lengths were used for the patterned substrates: a ‘long’ pattern with a length of 157.3 cm for measuring conductivities of pristine samples and those with a low oxidised content, and a ‘short’ pattern with a length of 37.2 cm for measuring more highly oxidised samples. The resistance across the channel was measured for all the blank slides, and any short circuits were discarded.

Thin films of our HTMs were deposited onto the patterned substrates from solution spin coating in an N_2 environment.

b. Spin coating films for conductivity

All solutions were prepared and kept in a N_2-filled glove box and were filtered before use. The solvent added to each vial was weighed on an electronic balance to account for errors associated with the micropipette calibration. Equivalent volumes were calculated using the solvent densities. The dopant solution was prepared as follows: 187.2 mg FK209 in 804.8 mg acetonitrile (182.83 mg/mL).

To prepare the HTM solutions for spin coating, one stock solution was prepared for each HTM studied, and then split into 7 vials of known solution mass. Each of these portions was

individually doped with increasing amounts of FK209 solution. Stock solutions were prepared as follows:

Spiro-OMeTAD: 39.2 mg spiro-OMeTAD in 2213.4 mg chlorobenzene (19.66 mg/mL).

EDOT-Amide-TPA (**1**): 18.4 mg EDOT-Amide-TPA in 1037.0 mg chlorobenzene + 1293.2 mg chloroform (10.2 mg/mL).

DEDOT-Amide-TPA (**2**): 17.2 mg DEDOT-Amide-TPA in 1016.0 mg chlorobenzene + 1428.1 mg chloroform (9.18 mg/mL)

TPABT (**3**): 52.6 mg TPABT in 602.5 mg chlorobenzene + 3269.5 mg chloroform (19.22 mg/mL).

The stock solutions were then split into separate vials, weighing the portion in each vial. and the doping volumes are given in Table S4. Solutions of compound **1** were kept on a hot plate at 70°C at all times to prevent precipitation, due to the significantly lower solubility of this material at room temperature compared to **2** and **3**. Doping was performed by adding known volumes of FK209 solution directly into the HTM vials which caused an immediate and strong colour change in all cases, as a result of the doping reaction forming the oxidised HTM.

Table S4: Measurements and doping equivalents for our conductivity experiment.

Spiro-OMeTAD Vial	**S1**	**S2**	**S3**	**S4**	**S5**	**S6**	**S7**
Stock solution mass (mg)	214.6	220.6	220.1	221.7	219.7	221.1	222.1
Added FK209 (µL)	1	3	5	7	9	12	15
mol%	**3.9**	**11.4**	**19.1**	**26.6**	**34.5**	**45.7**	**56.8**
EDOT-Amide-TPA Vial	**E1**	**E2**	**E3**	**E4**	**E5**	**E6**	**E7**
Stock solution mass (mg)	178.9	142.7	197.1	200.1	196.1	195.7	194.3
Added FK209 (µL)	1	2	4	5	6	7	8
mol%	**7.2**	**18.0**	**26.1**	**32.1**	**39.3**	**46.0**	**53.0**
DEDOT-Amide-TPA Vial	**D1**	**D2**	**D3**	**D4**	**D5**	**D6**	**D7**
Stock solution mass (mg)	218.3	232.3	207.4	222.2	228.1	232.2	223.4
Added FK209 (µL)	1	2	3	5	6	8	9
mol%	**6.8**	**12.8**	**21.6**	**33.6**	**39.2**	**51.4**	**60.1**
TPABT Vial	**T1**	**T2**	**T3**	**T4**	**T5**	**T6**	**T7**
Stock solution mass (mg)	246.0	240.4	283.9	251.5	246.6	250.7	244.0
Added FK209 (µL)	1	4	8	12	15	18	20

mol%	**2.8**	**11.6**	**19.6**	**33.2**	**42.3**	**49.9**	**57**

The mol% values in Table S4 were calculated based off of the concentrations of the HTM and dopant solutions, the number of moles of HTM in the transferred portion, and the number of moles of dopant in the added volume.

c. Pulsed J-V Measurement

The current-voltage characteristics of our HTMs were measured by a pulsed voltage setup whereby a range of voltages were randomly pulsed through our HTM films by means of a source meter, measuring the resulting current. The rapid pulsing of voltages, as opposed to a voltage sweep, has the effect of eliminating any effect of ionic conductivity, allowing us to selectively measure conductivity arising from the movement of holes.

To complete the conductivity calculation, film thicknesses were measured using a DekTak XT contact profiler equipped with a 2 μm stylus tip. Three separate valleys were etched into a thin film of each HTM on glass using a metal ruler and a cotton bud wetted with dichloromethane. The film thickness was then measured as the height difference across the etched valley. Three separate measurements across each valley allowed calculation of the film thickness as an average of 9 measurements across each film, as well as the standard deviation.

The conductivity of the samples was calculated by taking the inverse of the resistivity equation:

$$\sigma = \frac{l}{RA} \tag{8}$$

where σ = conductivity

R = resistance,

A = cross-sectional area through which conduction is occurring,

And l is the conduction length.

From our current-voltage curves, the resistance is extracted through calculating the gradient as 1/R, through Ohm's law (V = IR). Defining slope as 'S':

$$S = \frac{d(I)}{d(V)} = \frac{1}{R} \tag{9}$$

On our patterned slides, the conducting length is given by the channel width 'W'. The cross-sectional area is thus given by the product of the total length of the channel (L) and the film thickness (T). Substituting these terms, we get Equation 10:

$$\sigma = \frac{d(I)}{d(V)} \times \frac{W}{T \cdot L} = \frac{W}{T \cdot L \cdot R}$$

$$\sigma = \frac{W \cdot S}{T \cdot L}$$

(10)

Error bars were calculated for all of our data points using the error propagation equation:

$$\Delta f(x_i) = \sqrt{\sum_{x_i} \left(\frac{\partial f}{\partial x_i} \times \Delta x_i \right)^2} \quad (11)$$

Where Δf(x) is the error of a function comprised of a series of variables x_i, $\frac{\partial f}{\partial x_i}$ is the first partial derivative of the function with respect to each variable, multiplied by Δx_i, the error in each variable.

In our conductivity equation, there are three variables with associated error, these being:

1.) Channel width W: carries error ΔW which is the standard deviation of measured channel widths as measured using an optical microscope.
2.) Film thickness T: carries error ΔT which is the standard deviation of measured film thicknesses from the profilometer.
3.) Resistance R: carries error ΔR from the error of the fit of the IV characteristic graphs.

The channel length L is dictated by our pre-designed pattern and is taken to have negligible error, so it was not included in the derivation. Thus the propagated error equation becomes:

$$\Delta\sigma = \sqrt{\left(\frac{\partial \sigma}{\partial W} \times \Delta W \right)^2 + \left(\frac{\partial \sigma}{\partial T} \times \Delta T \right)^2 + \left(\frac{\partial \sigma}{\partial R} \times \Delta R \right)^2}$$

Solving partial derivatives, and substituting Equation 10:

$$\frac{\partial}{\partial W}\left(\frac{W \cdot S}{T \cdot L}\right) = \frac{S}{T \cdot L} = \frac{\sigma}{W}$$

$$\frac{\partial}{\partial T}\left(\frac{W \cdot S}{T \cdot L}\right) = -\frac{W \cdot S}{T^2 \cdot L} = -\frac{\sigma}{T}$$

$$\frac{\partial}{\partial R}\left(\frac{W \cdot S}{T \cdot L}\right) = -\frac{W \cdot S}{T \cdot L \cdot R} = -\frac{\sigma}{R}$$

Substituting:

$$\Delta\sigma = \sqrt{\left(\frac{\sigma}{W}\right)^2 \Delta W^2 + \left(-\frac{\sigma}{T}\right)^2 \Delta T^2 + \left(-\frac{\sigma}{R}\right)^2 \Delta R^2}$$

Simplifying,

$$\Delta\sigma = \sigma \sqrt{\left(\frac{\Delta W}{W}\right)^2 + \left(\frac{\Delta T}{T}\right)^2 + \left(\frac{\Delta R}{R}\right)^2}$$

$$\Delta\sigma = \sigma \sqrt{\left(\frac{\Delta W}{W}\right)^2 + \left(\frac{\Delta T}{T}\right)^2 + (S\Delta R)^2} \quad (12)$$

12. SCLC Measurements

HTM films for mobility measurements through the SCLC technique were prepared through solution spin coating, using concentrated solutions of the HTMs and slower spin coating speeds to ensure maximum thickness of the HTM film. “Hole-only” devices were then prepared with the following architecture: Fluorine-doped tin oxide (FTO) / HTM / Ag.[13] Current-voltage characteristics were then measured through similar methodology as used for conductivity measurements. Assuming Ohmic contacts, the current at higher voltages is taken to be space-charge limited. Carrier mobility was thus estimated by fitting to the Mott-Gurney law (Equation 13):[14]

$$J = \frac{9}{8}\varepsilon_0 \varepsilon_r \mu \frac{V^2}{L^3} \quad (13)$$

Here, **J** is the current density, ε_0 is the permittivity of free space, ε_r is the relative permittivity of the HTM, **μ** is the hole mobility, **V** is the applied voltage and **L** is the HTM film thickness. All film thicknesses were measured through AFM. Current density was estimated for a channel of area 0.26 mm^2. Relative permittivity is taken to be 3, which is common for most organic semiconductors.[15]

In order to prepare sufficiently thick films for SCLC measurements, concentrated solutions were prepared for spin coating according to the following measurements:

Spiro-OMeTAD: 120.0 mg spiro-OMeTAD in 571.5 mg chlorobenzene (233.1 mg/mL).

EDOT-Amide-TPA (**1**): 15.3 mg EDOT-Amide-TPA in 325.0 mg chlorobenzene + 857.6 mg chloroform (17.6 mg/mL).

DEDOT-Amide-TPA (**2**): 76.0 mg DEDOT-Amide-TPA in 441.7 mg chlorobenzene (191.0 mg/mL).

TPABT (**3**): 52.3 mg TPABT in 238.4 mg chlorobenzene + 294.4 mg chloroform (126.8 mg/mL).

Solutions of compounds **1** and **3** were kept at 70°C at all times to prevent precipitation of the HTM, ensuring good film formation. Films were deposited through static spin coating using slower spinning speeds to further increase film thickness (1000 rpm for 5 seconds, followed by 5000 rpm for 10 seconds). Film thicknesses were measured through AFM on a thin channel etched into the film with a razor.

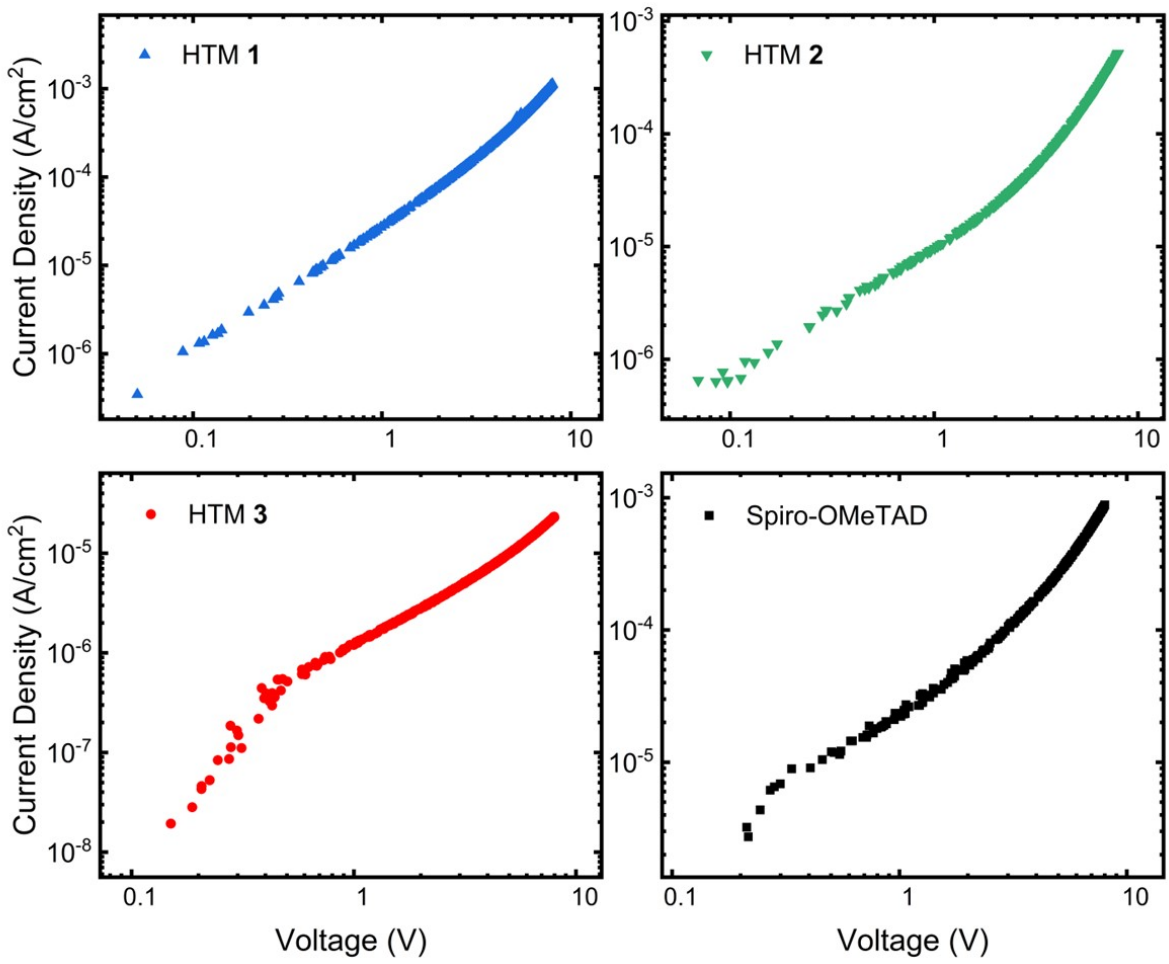

Figure S9: Current-density measurements of our three amide HTMs and spiro-OMeTAD, plotted on a log-log scale.

13. Perovskite solar cell fabrication

Synthesis of perovskite precursors

To prepare the methylammonium (**MAI**) crystals, methylamine (40% wt. in H_2O, 79.1 mL, 913.7 mmol) and hydriodic acid (without stabilisers, 55% wt. in H_2O, 50 mL, 365.5 mmol) were added to a round bottomed flask containing ethanol (300 mL) and stirred overnight, resulting in a colourless solution. Residual ethanol and water were removed through rotary evaporation, yielding a white, crystalline solid. The crude product was washed with diethyl ether, then recrystallised three times from dry ethanol, and washing with diethyl ether after each procedure to yield white crystals of the pure product (19.152 g, 33%). The triple-cation (**FAMACs**) perovskite solution was prepared by mixing 0.07M cesium iodide (CsI, TCI Chemicals), 0.08 M MAI, 1.32 M formamidinium iodide (FAI, Greatcell Solar), 1.54M lead (II) iodide (PbI_2, TCI Chemicals) and 0.5M methylammonium chloride (MACl, Merck) and dissolving them in a 4:1 v/v DMF:DMSO mixed solvent system.[16]

Solar Cell Fabrication

Substrates (FTO Glass) were washed with Hellmanex III 2 vol% in deionised (DI) water, rinsed with DI-water, acetone, ethanol and DI-water again, and finally dried with nitrogen. Substrates were treated with ozone for 20 minutes. A compact titanium oxide (TiO_2) electron transport layer was deposited via a sol-gel method. 370 µL of titanium (IV) isopropoxide (99.999%, Sigma-Aldrich) in 2.5 mL of IPA was mixed with 35 µL of 2M HCl in 2.5 mL of IPA under stirring. 300 µL of the TiOx solution was spincoated dynamically onto the substrates at 2000 rpm for 45s. The films were annealed at 150°C for 30 minutes, followed by 500°C for 45 minutes.

Substrates were then transferred into a nitrogen-filled glovebox, where a layer of C_{60}-SAM (4-(1',5'-Dihydro-1'-methyl-2'H-[5,6]fullereno-C_{60}-I_h-[1,9-c]pyrrol-2'-yl)benzoic acid, Sigma-Aldrich) (0.5 mg/mL in chlorobenzene) was deposited via spin coating 50 µL at 2000 rpm for 30 seconds, and annealed at 100°C for 10 minutes. A layer of Al_2O_3 nanoparticles (Sigma-Aldrich, 20 wt% in IPA, diluted to 0.16 wt% in IPA) was then deposited via spin coating 50 µL at 2000 rpm for 30 seconds, and annealed at 100°C for 10 minutes.[17]

The perovskite solution was deposited via a two-step spin coating process. 50 µL of solution was dynamically deposited onto the substrates during a 10 s, 1000 rpm step, followed by a 40 s 4000 rpm step. At the last 5 seconds of the second step, 300 µL of ethyl acetate antisolvent was deposited onto the substrate. The substrates were then annealed at 100°C for 45 minutes, and at 150°C for 10 minutes. A 2.5 mM solution of PEAI in IPA was then spincoated at 5000 rpm for 30 s, followed by annealing at 70°C for 5 minutes. The hole transport layers were prepared and deposited as follows:

Spiro-OMeTAD: A 80 mg/mL solution was prepared in chlorobenzene. 19 µL of LiTFSI solution (519 mg / mL in acetonitrile (ACN)), 14 µL of FK209 solution (374 mg/mL in ACN) and 34 µL of 4-tert-butylpyridine (tBP), then spincoated at 3000 rpm for 30 seconds.[16]

EDOT-Amide-TPA (HTM **1**): A 10 mg/mL solution in 4:1 v/v chlorobenzene : chloroform was dissolved at 100°C and mixed with 30 µL of LiTFSI solution (170 mg / mL in ACN), and 10 µL of tBP, then spincoated at 1000 rpm for 30 seconds and 2000 rpm for 5 seconds. The solution was kept at 70°C at all times during the preparation and spin coating process.[1]

DEDOT-Amide-TPA (HTM **2**): A 10 mg/mL solution in 4:1 v/v chlorobenzene : chloroform was mixed with 20 µL of LiTFSI solution (170 mg / mL in ACN), and 10 µL of tBP, then spincoated at 1000 rpm for 30 seconds and 2000 rpm for 5 seconds.

TPABT (HTM **3**): A 10 mg/mL solution in 2:1 v/v chlorobenzene : chloroform was mixed with 25 µL of LiTFSI solution (170 mg / mL in ACN), and 10 µL of tBP, then spincoated at 1250 rpm for 40 seconds and 2000 rpm for 5 seconds.[4]

Finally, 50 nm thick gold electrodes were deposited via thermal evaporation.

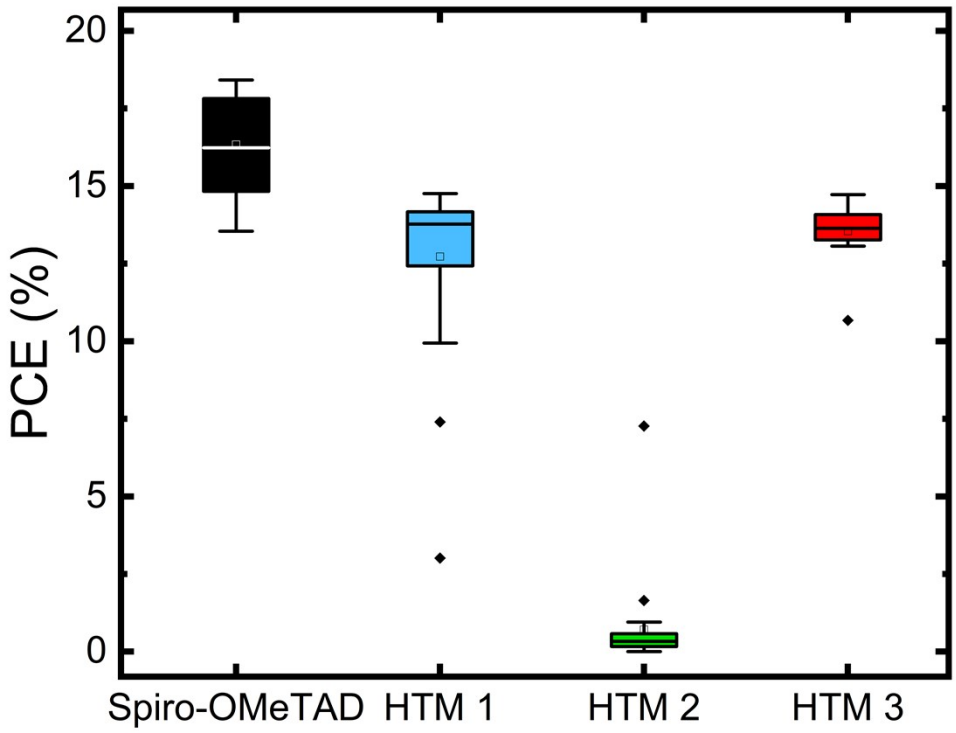

Figure S10: PCE distributions of our fabricated PSCs.

14. References

1 M. L. Petrus, K. Schutt, M. T. Sirtl, E. M. Hutter, A. C. Closs, J. M. Ball, J. C. Bijleveld, A. Petrozza, T. Bein, T. J. Dingemans, T. J. Savenije, H. Snaith and P. Docampo, *Adv. Energy Mater.*, 2018, **8**, 1–11.

2 G. S. Liou and C. W. Chang, *Macromolecules*, 2008, **41**, 1667–1674.

3 M. L. Petrus, T. Bein, T. J. Dingemans and P. Docampo, *J. Mater. Chem. A*, 2015, **3**, 12159–12162.

4 E. A. A. Alkhudhayr, D. Sirbu, M. Fsadni, B. Vella, B. T. Muhammad, P. G. Waddell, M. R. Probert, T. J. Penfold, T. Hallam, E. A. Gibson and P. Docampo, *ACS Appl. Energy Mater.*, 2023, 11573–11582.

5 T. P. Osedach, T. L. Andrew and V. Bulović, *Energy Environ. Sci.*, 2013, **6**, 711–718.

6 Merck, https://www.sigmaaldrich.com/GB/en, (accessed 29 May 2024).

7 M. L. Petrus, A. Music, A. C. Closs, J. C. Bijleveld, M. T. Sirtl, Y. Hu, T. J. Dingemans, T. Bein and P. Docampo, *J. Mater. Chem. A*, 2017, **5**, 25200–25210.

8 F. Neese, *WIREs Comput Mol Sci*, 2012, **2**, 73–78.

9 T. J. Pope, T.; Giret, Y.; Fsadni, M.; Docampo, P.; Groves, C.; Penfold, *Org. Electron.*, 2023, **115**, 106760 (1–6).

10 W. J. Chi, Q. S. Li and Z. S. Li, *Nanoscale*, 2016, **8**, 6146–6154.

11 E. Speckmeier, T. G. Fischer and K. Zeitler, *J. Am. Chem. Soc.*, 2018, **140**, 15353–15365.

12 W. H. Nguyen, C. D. Bailie, E. L. Unger and M. D. McGehee, *J. Am. Chem. Soc.*, 2014, **136**, 10996–11001.

13 P. Huang, A. Hernández, S. Kazim, J. Ortiz, Á. Sastre-Santos and S. Ahmad, *Sustain. Energy Fuels*, 2020, **4**, 6188–6195.

14 J. Nelson, *The Physics of Solar Cells*, Imperial College Press, 2003.

15 H. J. Snaith and M. Grätzel, *Appl. Phys. Lett.*, , DOI:10.1063/1.2424552.

16 J. Petrulevicius, Y. Yang, C. Liu, M. Steponaitis, E. Kamarauskas, M. Daskeviciene, A. S. R. Bati, T. Malinauskas, V. Jankauskas, K. Rakstys, M. G. Kanatzidis, E. H. Sargent and V. Getautis, *ACS Appl. Mater. Interfaces*, 2024, **16**, 7310–7316.

17 M. Schultes, N. Giesbrecht, J. Küffner, E. Ahlswede, P. Docampo, T. Bein and M. Powalla, *ACS Appl. Mater. Interfaces*, 2019, **11**, 12948–12957.